

# Journal of Materials Chemistry A

Accepted Manuscript



This is an *Accepted Manuscript*, which has been through the Royal Society of Chemistry peer review process and has been accepted for publication.

*Accepted Manuscripts* are published online shortly after acceptance, before technical editing, formatting and proof reading. Using this free service, authors can make their results available to the community, in citable form, before we publish the edited article. We will replace this *Accepted Manuscript* with the edited and formatted *Advance Article* as soon as it is available.

You can find more information about *Accepted Manuscripts* in the [Information for Authors](#).

Please note that technical editing may introduce minor changes to the text and/or graphics, which may alter content. The journal's standard [Terms & Conditions](#) and the [Ethical guidelines](#) still apply. In no event shall the Royal Society of Chemistry be held responsible for any errors or omissions in this *Accepted Manuscript* or any consequences arising from the use of any information it contains.

Cite this: DOI: 10.1039/c0xx00000x

www.rsc.org/xxxxxx

ARTICLE TYPE

# Facile template-free synthesis of 3D porous MnO/C microspheres with controllable pore size for high-performance lithium-ion battery anodes

Kai Su,<sup>a</sup> Chao Wang,<sup>b</sup> Honggang Nie,<sup>a</sup> Yan Guan,<sup>a</sup> Feng Liu<sup>\*a</sup> and Jitao Chen<sup>\*a</sup>

Received (in XXX, XXX) Xth XXXXXXXXX 20XX, Accepted Xth XXXXXXXXX 20XX

DOI: 10.1039/b000000x

The 3D porous MnO/C anode materials with controllable pore size are rationally designed and synthesized by a facile template-free strategy. The  $Mn_xZn_{1-x}CO_3$  ( $x=1, 2/3, 1/2, \text{ and } 1/3$ ) precursors are prepared by the ultrasonic-assisted co-precipitation method, and then heated with glucose in a reducing atmosphere to obtain a series of MnO/C microspheres through the topochemical conversion. These MnO/C microspheres consist of nanosized primary particles and have the interconnected pore architectures with high specific surface areas of up to  $111.4 \text{ m}^2 \text{ g}^{-1}$ . Adjusting the Zn/Mn molar ratio of  $Mn_xZn_{1-x}CO_3$  can easily tune the pore size of MnO/C materials from 14.9 to 31.8 nm. Electrochemical performances of MnO/C materials are found to be strongly correlated with porous structures. The MnO/C material with optimized pore size exhibits a high reversible capacity ( $846 \text{ mAh g}^{-1}$  at  $100 \text{ mA g}^{-1}$ ), superior rate capability ( $406 \text{ mAh g}^{-1}$  at  $3200 \text{ mA g}^{-1}$ ), and excellent cycling stability. This strategy can be extended to prepare other candidate electrode materials.

## Introduction

Lithium-ion batteries (LIBs) as one of the most promising power sources have attracted much attention due to the growing market demand for portable electronic devices and electric vehicles.<sup>1,2</sup> Tremendous efforts have been made to develop electrode materials to improve the performance of LIBs.<sup>3-5</sup> In the last decade, transition metal compounds have been explored as anode materials.<sup>6-11</sup> Among them, MnO is admirable due to its high theoretical capacity ( $756 \text{ mAh g}^{-1}$ ), low cost, environmental benignity, high density ( $5.43 \text{ g cm}^{-3}$ ), and low electrochemical motivation force ( $1.032 \text{ V vs. Li}^+/\text{Li}$ ).<sup>12-25</sup> However, the conversion reaction during the lithium storage causes drastic volume change, leading to severe pulverization of particles and loss of the electronic contact.<sup>13</sup> In addition, MnO anode materials suffer from poor rate capability as a result of kinetic limitations.<sup>13,25</sup>

Recently, the porous structure is quite attractive in the design of MnO materials owing to its advantages of relieving the volume change in the electrochemical reaction and increasing the contact area between the active material and the electrolyte.<sup>13-21</sup> Despite some achievements have been made, these existing uncontrolled porous structures are unable to meet the requirement for further optimizing the electrochemical performance of MnO anode materials. It is well known that the pore size and the distribution of pores in porous configuration largely determine the electrochemical performance of materials.<sup>26,27</sup> The ideal void space can maintain the structure of materials for good cycling stability without wasting volume in porous electrodes. Moreover, the well-defined porous structure would possess the nanosized features, high specific surface area and appropriate pore size, which can improve the rate performance of materials. To the best

of our knowledge, no report has focused on synthesis of 3D porous micrometer-sized MnO materials with controllable pore size, and the effect of pore size on the electrochemical performance of MnO materials.

It is quite a challenge to prepare a series of porous materials with controllable pore size. Up to now, several strategies including templating and template-free methods are developed to regulate the pore size in the fabrication of porous materials. KIT-6 and SBA-15 have been used as the hard templates to synthesize ordered mesoporous materials with various pore sizes.<sup>28,29</sup> Template-free protocols, such as chemical etching,<sup>30</sup> thermal decomposition,<sup>31</sup> solvothermal,<sup>32</sup> anodization,<sup>33</sup> and sol-gel,<sup>34</sup> have also been attempted to tune the pore size of materials. However, most of the current approaches have the disadvantages of high cost, tedious synthetic steps, or limited controllability. Therefore, it remains necessary and meaningful to develop a simple strategy towards the synthesis of 3D porous materials with controllable pore size for effectively optimizing the electrochemical performance.

Herein, for the first time, we report a facile template-free strategy by combining the ultrasonic-assisted co-precipitation and the topochemical conversion to synthesize the 3D porous MnO/C microspheres with controllable pore size for high-performance lithium-ion battery anodes. The  $Mn_xZn_{1-x}CO_3$  ( $x=1, 2/3, 1/2, \text{ and } 1/3$ ) microspheres as the precursors were first prepared by the co-precipitation method with the aid of ultrasonic. Then, the mixture of precursor and glucose was heated in a reducing atmosphere to obtain a series of porous MnO/C microspheres through the topochemical conversion. We investigated the influence of the Zn/Mn molar ratio of the precursors on the physical and electrochemical behaviors of the resultant MnO/C materials in

detail. The results confirm the rationality of this strategy for controllable synthesis of porous MnO/C materials and the feasibility of tuning electrochemical performance. This work provides a simple and universal strategy to prepare other electrode materials with porous structure and controllable pore size for advanced lithium-ion batteries.

## Experimental section

### Synthesis of $Mn_xZn_{1-x}CO_3$ ( $x=1, 2/3, 1/2$ , and $1/3$ ) precursors

The mixed solutions of  $MnSO_4$  and  $ZnSO_4$  for  $MnCO_3$ ,  $Mn_{2/3}Zn_{1/3}CO_3$ ,  $Mn_{1/2}Zn_{1/2}CO_3$ , and  $Mn_{1/3}Zn_{2/3}CO_3$ , were prepared by adding  $MnSO_4 \cdot H_2O$  (1.77, 1.18, 0.89, and 1.77 g) and  $ZnSO_4 \cdot 7H_2O$  (0, 1.01, 1.51, and 6.02 g) to deionized water (700 mL), respectively. The  $NH_4HCO_3$  solutions for  $MnCO_3$ ,  $Mn_{2/3}Zn_{1/3}CO_3$ ,  $Mn_{1/2}Zn_{1/2}CO_3$  and  $Mn_{1/3}Zn_{2/3}CO_3$  were prepared by dissolving  $NH_4HCO_3$  (8.31, 8.31, 12.47, and 24.93 g) in deionized water (700 mL), respectively. Then  $NH_4HCO_3$  solution was poured into the mixed solution of  $MnSO_4$  and  $ZnSO_4$ , which was placed in the ultrasonic bath. The precipitation process was continued for 8 h. The obtained precipitates were washed three times by deionized water and dried in air at 80 °C overnight. Here the concentrations of the  $MnSO_4$ - $ZnSO_4$  mixed solution and the  $NH_4HCO_3$  solution are varied for synthesizing the  $Mn_xZn_{1-x}CO_3$  precursors with the similar diameter.

### Synthesis of MnO/C composites

$MnCO_3$  (0.6 g),  $Mn_{2/3}Zn_{1/3}CO_3$  (0.6 g),  $Mn_{1/2}Zn_{1/2}CO_3$  (0.6 g), or  $Mn_{1/3}Zn_{2/3}CO_3$  (0.6 g) was mixed with glucose (0.1, 0.12, 0.13, or 0.14 g) in deionized water (2 mL), respectively. Then the solutions were evaporated in air at 80 °C to obtain the white powders. These mixtures were put in the porcelain boat and heated at 650 °C in the 5%  $H_2/N_2$  atmosphere for 5 h to obtain the MnO/C composites. Here the quantity of glucose is varied for the synthesis of the composites with the similar carbon content.

### Characterization

The crystal structures of  $Mn_xZn_{1-x}CO_3$  precursors and MnO/C composites were identified by a D/max2400 power X-ray diffractometer (XRD) (Rigaku, Japan) with Cu-K $\alpha$  radiation ( $\lambda=1.5405 \text{ \AA}$ ) in a  $2\theta$  range of 10–80°. The morphologies of the prepared materials were observed with an S-4800 scanning electron microscope (SEM) (Hitachi, Tokyo, Japan) and a Tecnai G2 F20 transmission electron microscope (TEM) (FEI, Portland, USA). Focused ion beam (FIB) (FEI, Portland, USA) was applied to analyze the cross-sections of MnO/C composites. Carbon contents of MnO/C composites were determined by a Vario EL III elemental analyzer (Elementar, Germany). An ASAP2010 apparatus (Micromeritics, USA) was employed to investigate the pore structures and the specific surface areas of MnO/C composites.

### Electrochemical measurements

The electrochemical experiments were performed using 2032 coin-type cells. The working electrode consisted of 80 wt% active material (MnO/C composites), 10 wt% conductive carbon black,

and 10 wt% carboxyl methyl cellulose (CMC) as the binder. The electrolyte was a solution of 1 M  $LiPF_6$  in ethyl carbonate/dimethyl carbonate (EC/DMC) (1:1, v/v). Pure Li foil was used as the reference and counter electrode. The charge/discharge measurements were carried out in the voltage window from 0.01 to 3.0 V using a Land battery test system. The cyclic voltammetry measurements were performed on a CHI660D electrochemical station (Chenhua, Shanghai, China).

## Results and discussion

### Rational of design strategy for synthesis of porous MnO/C microspheres with controllable pore size

A facile template-free strategy, combining the ultrasonic-assisted co-precipitation and the topochemical conversion, is designed to synthesize 3D porous MnO/C microspheres with controllable pore size, as illustrated in Fig. 1. Firstly, the  $Mn_xZn_{1-x}CO_3$  precursor microspheres are prepared by the precipitation process which is carried out in an ultrasonic bath after the  $NH_4HCO_3$  solution is poured into the mixed solution of  $ZnSO_4$  and  $MnSO_4$ . Subsequently, glucose as the carbon source is mixed with the  $Mn_xZn_{1-x}CO_3$  precursor in water. During the following heat treatment at 650 °C in the 5%  $H_2/N_2$  reducing atmosphere, the mixture of  $Mn_xZn_{1-x}CO_3$  and glucose is decomposed to the composites of MnO/C and ZnO/C in the first stage, resulting in the formation of pores in the microspheres. In the second stage of the topochemical conversion, the reduction of ZnO and concurrent vapor-phase leaching of Zn further create the voids in situ. Finally, a series of 3D porous micrometer-sized MnO/C spheres with controllable pore size are obtained through adjusting the Zn/Mn molar ratio of  $Mn_xZn_{1-x}CO_3$  precursors.

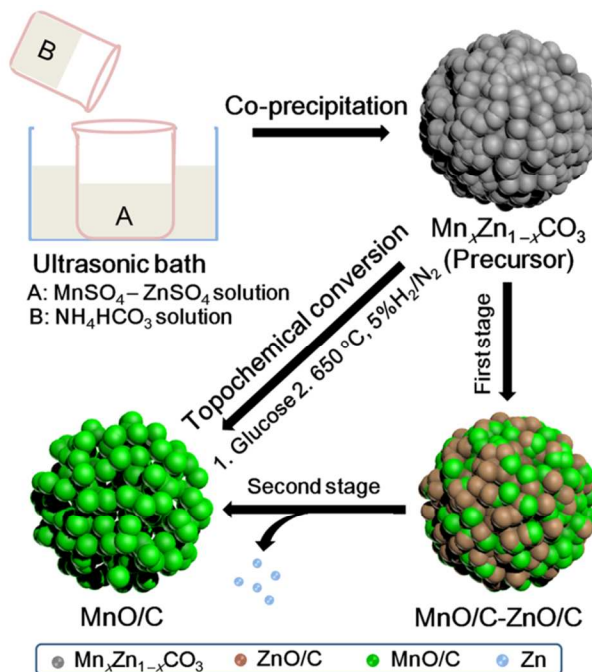


Fig. 1 Schematic representation of the design strategy for synthesis of 3D porous MnO/C microspheres with controllable pore size.

Cite this: DOI: 10.1039/c0xx00000x

www.rsc.org/xxxxxx

ARTICLE TYPE

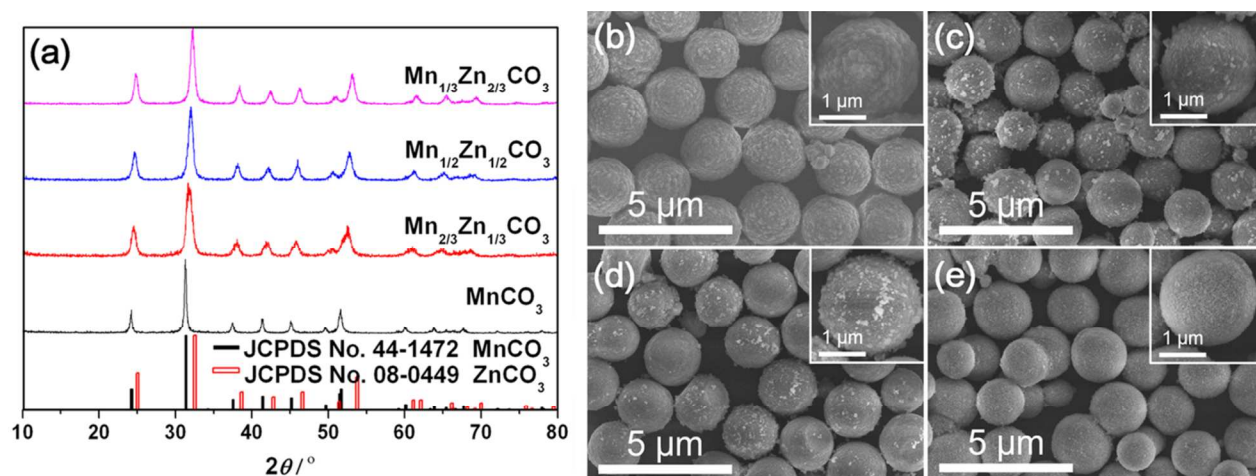


Fig. 2 XRD patterns of  $Mn_xZn_{1-x}CO_3$  ( $x=1, 2/3, 1/2,$  and  $1/3$ ) precursors (a), and SEM images of  $MnCO_3$  (b),  $Mn_{2/3}Zn_{1/3}CO_3$  (c),  $Mn_{1/2}Zn_{1/2}CO_3$  (d), and  $Mn_{1/3}Zn_{2/3}CO_3$  (e).

### Crystal structures and morphologies of $Mn_xZn_{1-x}CO_3$ ( $x=1, 2/3, 1/2,$ and $1/3$ ) precursors

The X-ray diffraction (XRD) patterns (Fig. 2a) present the crystallographic structures of four  $Mn_xZn_{1-x}CO_3$  precursors. The diffraction peaks of these precursors can be indexed as a hexagonal structure with a  $R\bar{3}c$  space group corresponding to  $MnCO_3$  (JCPDS No. 44-1472). The peak positions of  $Mn_xZn_{1-x}CO_3$  ( $x=2/3, 1/2,$  and  $1/3$ ) are just located between those of  $MnCO_3$  and  $ZnCO_3$ , and shift to higher  $2\theta$  values with the increase in the Zn/Mn molar ratio of the precursors. The results indicate these precursors are the solid solutions of  $MnCO_3$  and  $ZnCO_3$ .

The scanning electron microscope (SEM) images of  $Mn_xZn_{1-x}CO_3$  ( $x=1, 2/3, 1/2,$  and  $1/3$ ) (Fig. 2b–e) show that these precursor materials are composed of microspheres with a uniform

distribution and the average diameter around  $2\ \mu m$ . The corresponding high-magnification SEM images of these microspheres (Fig. 2b–e, insets) illustrate that the precursor microspheres have rough surfaces and consist of primary nanoparticles. From the control experiment where  $Mn_{2/3}Zn_{1/3}CO_3$  was prepared without the aid of ultrasonic, the aggregates and irregular-shaped particles are found in this precipitate (Fig. S1). It is confirmed that the ultrasonic in the co-precipitation process plays a vital role in the formation of  $Mn_xZn_{1-x}CO_3$  microspheres with a high uniformity.

### Crystal structures and morphologies of MnO/C composites

Fig. 3a displays the XRD patterns of four MnO/C composites (described as MnO/C-1, MnO/C-2, MnO/C-3, and MnO/C-4) prepared from the corresponding  $Mn_xZn_{1-x}CO_3$  ( $x=1, 2/3, 1/2,$  and

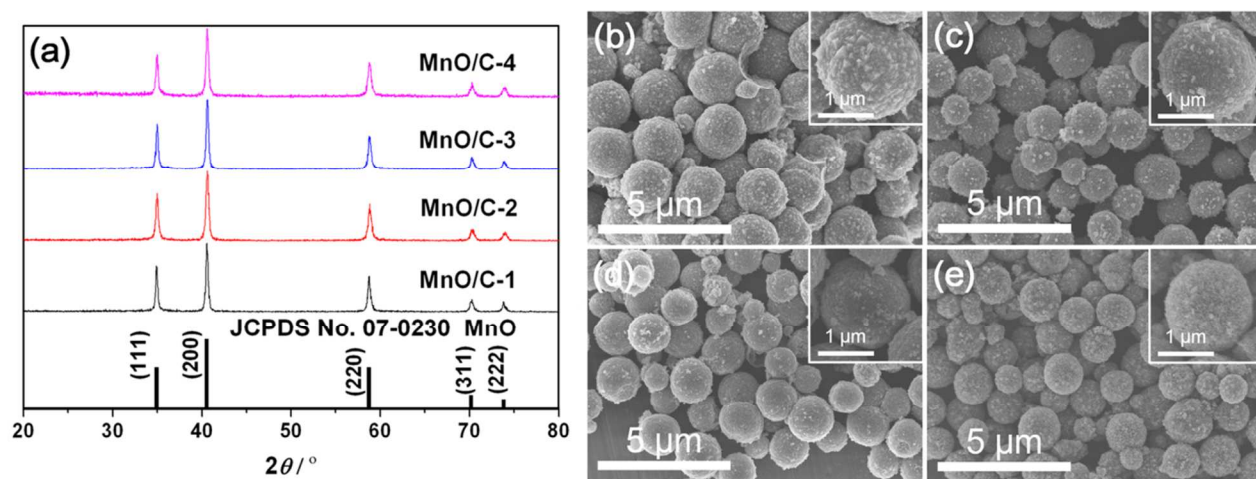


Fig. 3 XRD patterns of four MnO/C composites (a), and SEM images of MnO/C-1 (b), MnO/C-2 (c), MnO/C-3 (d), and MnO/C-4 (e).

Cite this: DOI: 10.1039/c0xx00000x

www.rsc.org/xxxxxx

## ARTICLE TYPE

1/3) precursors, respectively. All the peaks of these products can be indexed as a cubic phase of MnO with a space group of  $Fm\bar{3}m$  (225) (JCPDS No. 07-0230). The five diffraction peaks located at  $2\theta=34.9^\circ$ ,  $40.5^\circ$ ,  $58.7^\circ$ ,  $70.2^\circ$ , and  $73.8^\circ$  are assigned to the (111), (200), (220), (311), and (222) lattice planes of MnO, respectively. No impurity phase is found. The crystal sizes of MnO/C composites are estimated by using the Scherrer's equation based on the half-width of the (200) reflection. These composites have the similar crystal sizes as the calculated crystallite sizes of MnO/C-1, -2, -3, and -4 are 38, 30, 33, and 31 nm, respectively. It is noticed that the Zn/Mn molar ratio of the precursors has little impact on the crystal size of the resultant MnO/C composites. In the topochemical conversion, the annealing conditions (temperature and time) are crucial for the remove of  $ZnCO_3$  and the maintenance of porous network. As shown in Fig. S2, short annealing time and low heating temperature are not beneficial for removing  $ZnCO_3$ , while high temperature causes the shrinkage and the solidification of microspheres (Fig. S3), resulting in a large decrease of porosity.<sup>35</sup> The optimal heating temperature and annealing time are  $650^\circ\text{C}$  and 5 h, respectively.

Fig. 3b–e present the SEM images of four MnO/C composites. As displayed in Fig. 3b–e, these composites have similar morphologies with the precursors, indicating that the spherical morphologies are perfectly kept after the calcination process. The average diameter of MnO/C microspheres is about 1.5  $\mu\text{m}$  and slightly smaller than that of the corresponding precursors. The high-magnification SEM images (Fig. 3b–e, insets) show that these microspheres remain rough surfaces and consist of nanosized subunits. The carbon contents of MnO/C-1, -2, -3, and -4 composites, determined by the elemental analyzer, are 6.51%, 5.18%, 5.71%, and 5.35%, respectively. Fig. S4 depicts the SEM images of bare MnO sample prepared from  $Mn_{1/2}Zn_{1/2}CO_3$  precursor in the absence of glucose. The broken microspheres are found in this MnO sample. Meanwhile, the primary particle size is larger than that of MnO/C-3. Therefore, the carbon coating assists the preservation of the spherical morphology of MnO/C composites during the topochemical conversion. The growth of primary particles is also restricted by the carbon coating to shorten the diffusion distance of  $Li^+$  for the improvement of the rate capability of MnO/C composites.

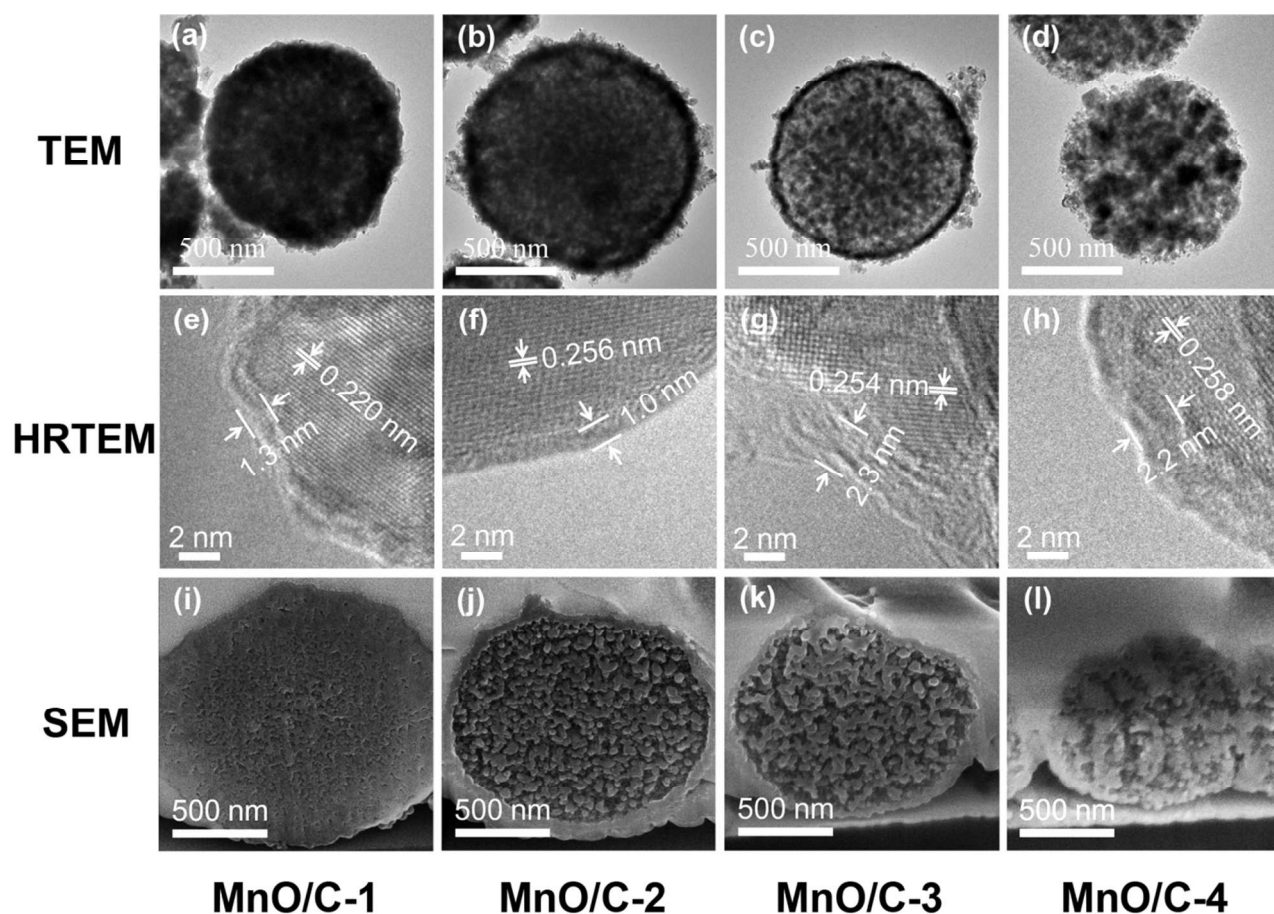


Fig. 4 TEM, HRTEM, cross-sectional SEM images of MnO/C microspheres.

Cite this: DOI: 10.1039/c0xx00000x

www.rsc.org/xxxxxx

## ARTICLE TYPE

## Porous structures of MnO/C microspheres

The transmission electron microscope (TEM) is applied to examine the structures and crystallographic characteristics of MnO/C microspheres. As seen in Fig. 4a–d, the pore volume in the MnO/C microspheres obviously is increased with increasing the Zn/Mn molar ratio of the precursors from 0 to 2, while porous network architectures are formed inside these microspheres. The results confirm that ZnCO<sub>3</sub> in the precursors acts as the porogen to successfully generate more voids in the microspheres through the topochemical conversion. In comparison with the uniformly distributed pores in the other MnO/C composites, the porous structure of the MnO/C-4 microsphere possesses randomly distributed pores and some aggregated nanoparticles. Fig. 4e–h depict the high resolution TEM (HRTEM) images taken from the outside edges of four MnO/C composites. The atomic layers of MnO/C-1, -2, -3, and -4 have the d-spacing values of 0.220, 0.256, 0.254, and 0.258 nm, which are assigned to the (200), (111), (111), and (111) reflections of MnO, respectively. Moreover, the surfaces of MnO crystals are uniformly covered by an amorphous carbon coating of 1–3 nm.

The cross-sectional SEM images of MnO/C microspheres (Fig. 4i–l) clearly display the internal nanostructures of MnO/C composites. These MnO/C composites present abundant nanosized pores which distribute throughout the micrometer-sized MnO/C spheres. The primary nanoparticles are connected with each other to form the 3D network. In coincidence with the TEM results (Fig. 4a–d), MnO/C composite has an obvious increase in the pore size with increasing the Zn/Mn molar ratio of the precursors. The results confirm the rationality of presented strategy for the synthesis of well-defined porous MnO/C composites and the control of porous structure by adjusting the Zn/Mn molar ratio of the precursors.

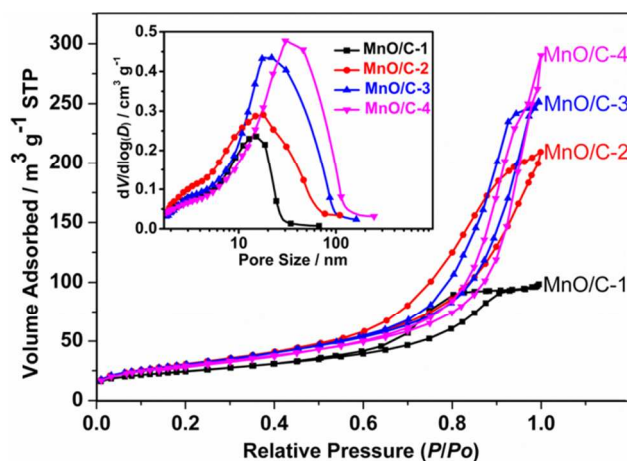


Fig. 5 Nitrogen adsorption-desorption isotherms for four MnO/C composites, the inset shows the corresponding pore size distributions.

Table 1 Physical properties from N<sub>2</sub> sorption studies of porous MnO/C microspheres.

Sample	Pore size (nm)	Pore volume (cm <sup>3</sup> g <sup>-1</sup> )	Specific surface area (m <sup>2</sup> g <sup>-1</sup> )
MnO/C-1	14.9	0.152	85.0
MnO/C-2	17.5	0.324	111.4
MnO/C-3	21.0	0.389	109.7
MnO/C-4	31.8	0.449	104.6

The pore structures and the Brunauer-Emmett-Teller (BET) surface areas of MnO/C composites were further investigated by the nitrogen sorption technique. As shown in Fig. 5, these MnO/C composites exhibit the typical IV isotherms along with the obvious H2 hysteresis loops, indicating the presence of pores in these samples. The corresponding pore size distributions of MnO/C composites, which are derived from the adsorption branches, are illustrated in the inset of Fig. 5. The physical properties of four MnO/C microspheres are listed in Table 1. While the Zn/Mn molar ratio is increased from 0 to 2, the pore size of the resultant MnO/C composites can be tuned from 14.9 to 31.8 nm. Accordingly, the pore volumes of MnO/C composites also can be regulated in the range from 0.152 to 0.449 cm<sup>3</sup> g<sup>-1</sup>. The increasing trends in the pore size and the pore volume are in accordance with the TEM and SEM images in Fig. 4. Additionally, MnO/C-1, -2, -3, and -4 have the high specific surface areas of 85.0, 111.4, 109.7, and 104.6 m<sup>2</sup> g<sup>-1</sup>, respectively. In comparison with those reported MnO materials (Table S1), four MnO/C composites all have higher specific surface areas owing to 3D porous architectures. It is revealed that the regulating element, the Zn/Mn molar ratio of the precursors, can be used to tune the physical properties of MnO/C microspheres.

## Electrochemical performances of the porous MnO/C materials

We investigated the impact of the porous structure on electrochemical properties of MnO/C materials in detail. Fig. 6a presents the cycling performances of four MnO/C materials at the charge and discharge current densities of 200 and 800 mA g<sup>-1</sup>, respectively. It is found that the capacity of MnO/C-1 decays with cycling, and MnO/C-2 also displays a decreasing capacity when the capacity reaches to the maximum value. The reversible capacities of MnO/C-3 and MnO/C-4 increase gradually within the initial 30 cycles, and then remain stable in the following cycles. The capacity increase of MnO/C-3 and -4, which is consistent with the increasing peak intensity in the corresponding CV curves (Fig. S5), is mainly ascribed to the activation of the electrode materials<sup>21,36,37</sup> and the formation of higher oxidation state products (Fig. S6).<sup>18,25</sup> After 100 cycles, the capacities of MnO/C-1, -2, -3, and -4 are retained 68.2%, 94.5%, 110.1%, and 121.0% of the corresponding second cycle discharge capacities, respectively. The SEM and TEM are applied to further examine the morphologies of MnO/C materials after 100 cycles and explore the impact of the structure stability on the cycling

30 865, 846, and 813 mAh g<sup>-1</sup>, respectively. When the current

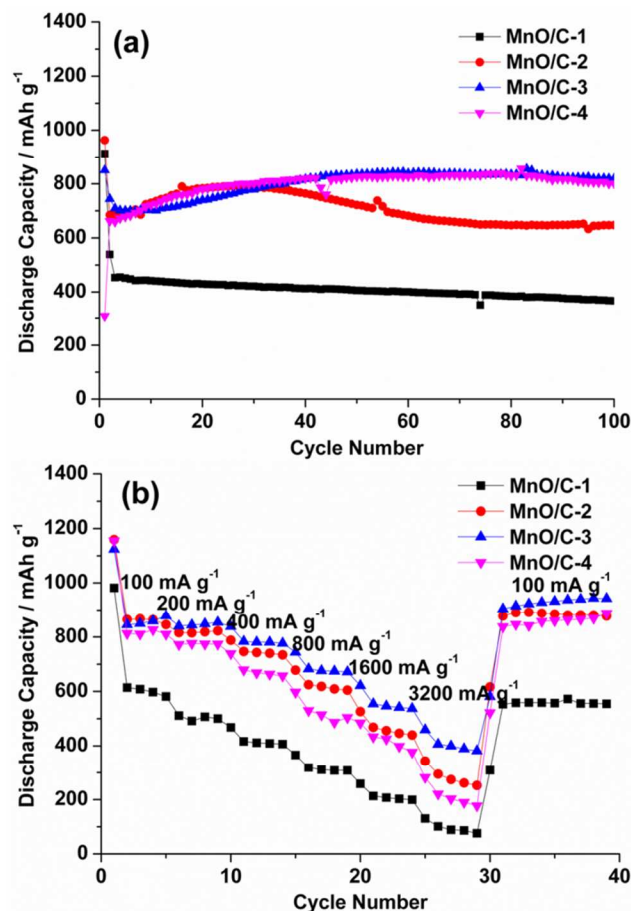


Fig. 6 Cycling stability (a) and rate capability (b) of four MnO/C materials. The cycling behaviors are tested at the charge and discharge current densities of 200 and 800 mA g<sup>-1</sup>, respectively.

of materials. Fig. 7a,b show that the microspheres of MnO/C-1 and MnO/C-2 collapse after intensive cycling. It is supposed that the void spaces in MnO/C-1 and MnO/C-2 are not large enough to reversibly accommodate the volume change during lithiation and delithiation, leading to the fracture and pulverization of microspheres. Instead, the original spherical shapes of MnO/C-3 and MnO/C-4 are preserved (Fig. 7c,d) as the higher porosities prevent the volume expansion and contraction of materials. Meanwhile, as shown in Fig. 7e,f, the internal porous structures of MnO/C-3 and MnO/C-4 are still kept, indicating the insertion and extraction of lithium ion have little impact on the porous structures. Therefore, the larger void space contributes to the superior structure stability of 3D porous materials, giving rise to the excellent cycling stability.

The rate capabilities of four MnO/C materials with various pore sizes are shown in Fig. 6b. MnO/C-1 displays the relatively lower specific discharge capacities at the current densities of 100–3200 mA g<sup>-1</sup>. It is supposed that the small pores of MnO/C-1 cause a restricted access of the electrolyte to active material. While increasing the Zn/Mn molar ratio of precursors from 0.5 to 2, the resultant MnO/C-2, -3, and -4 with enlarged pore size have the obvious increase in the reversible specific capacities due to the improved electrolyte transport. At low current density of 100 mA g<sup>-1</sup>, MnO/C-2, -3, and -4 have the high specific capacities of

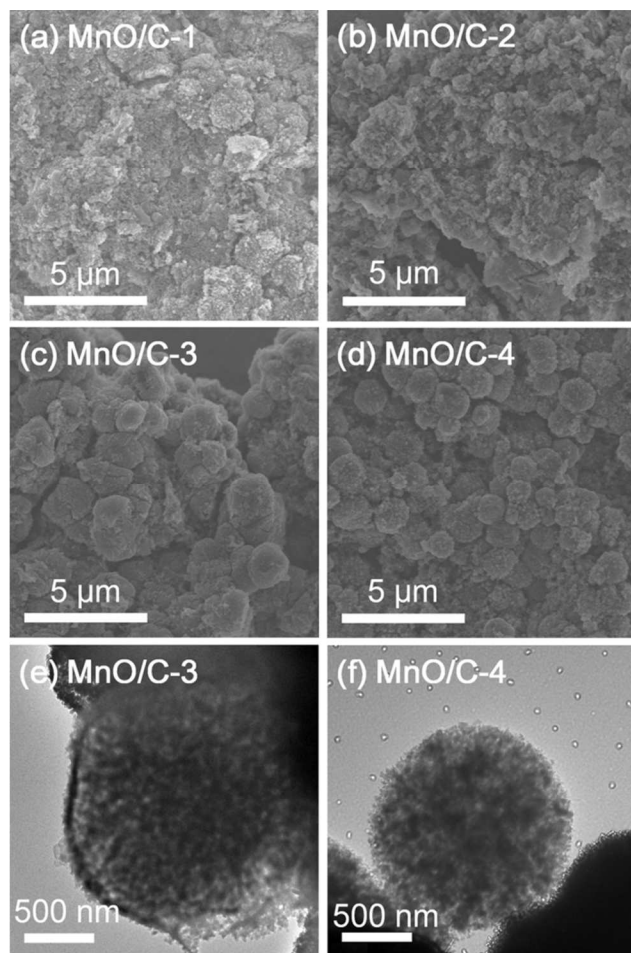


Fig. 7 SEM (a–d) and TEM (e, f) images of MnO/C composites after 100 cycles.

density increases to 3200 mA g<sup>-1</sup>, MnO/C-2, -3, and -4 exhibit the specific capacities of 295, 406, and 221 mAh g<sup>-1</sup>, respectively. MnO/C-3 shows the best rate performance as the stable porous structure and the appropriate pore size can facilitate Li<sup>+</sup> transport in the electrolyte phase. The results reveal that the pulverization of MnO/C-2 microspheres (Fig. 7b) has a negative influence on the electrolyte diffusion. It is also demonstrated that the aggregation of particles (Fig. 4i) deteriorates the rate capability though MnO/C-4 with larger pore size provides more void space as the reservoir for lithium ions. Therefore, the 3D porous network of MnO/C-3 with nanosized primary particles, high specific surface area, and optimized pore size makes the most efficient enhancement in the rate performance. The rate capability of MnO/C-3 is superior among those of the reported MnO materials (Table S2). The research results prove that the electrochemical performance of MnO/C materials can be effectively controlled by tuning the pore size of materials.

## Conclusions

In this work, we successfully developed a novel template-free strategy to prepare the 3D porous MnO/C microspheres with controllable pore size. The Zn/Mn molar ratio of Mn<sub>x</sub>Zn<sub>1-x</sub>CO<sub>3</sub> precursors is a crucial regulating element to achieve the

Cite this: DOI: 10.1039/c0xx00000x

www.rsc.org/xxxxxx

## ARTICLE TYPE

formation of tunable 3D porous network in MnO/C microspheres for controlling the electrochemical performances of MnO anode materials. MnO/C-3 exhibits the superior rate capability and excellent cycling stability, which is ascribed to the unique stable porous architecture with nanosized features and optimized pore size. We anticipate that our strategy can also be applied to prepare a series of other candidate electrode materials with controllable pore size for high-performance lithium ion batteries.

## Acknowledgements

This work was financially supported by the National Natural Science Foundation of China (21035005 and 21275013) and the Ministry of Science and Technology of China (2013AA110102). We are grateful to Prof. C. Z. Gu's group in Institute of Physics Chinese Academy of Sciences for the use of FIB equipment.

## Notes and references

<sup>a</sup>Beijing National Laboratory for Molecular Sciences, Key Laboratory of Bioorganic Chemistry and Molecular Engineering of Ministry of Education, College of Chemistry, Peking University, Beijing 100871, China. Fax: +86-10-62751708; Tel: +86-10-62761187; Email: liufeng@pku.edu.cn; chenjitao@pku.edu.cn

<sup>b</sup>College of Materials Science and Engineering, Huazhong University of Science and Technology, Wuhan 430074, China.

† Electronic Supplementary Information (ESI) available: The morphology images and XRD patterns of samples prepared in the synthetic optimization, cyclic voltammograms of MnO/C materials, tables of BET surface areas, pore sizes and electrochemical performances of the reported MnO anode materials. See DOI: 10.1039/b000000x/

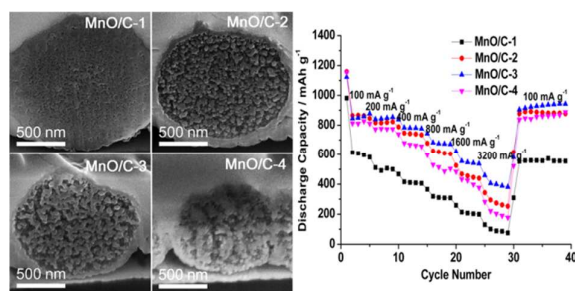
- 1 J. M. Tarascon and M. Armand, *Nature*, 2001, **414**, 359–367.
- 2 V. Etacheri, R. Marom, R. Elazari, G. Salitra and D. Aurbach, *Energy Environ. Sci.*, 2011, **4**, 3243–3262.
- 3 P. G. Bruce, B. Scrosati and J. M. Tarascon, *Angew. Chem. Int. Ed.*, 2008, **47**, 2930–2946.
- 4 H. Li, Z. X. Wang, L. Q. Chen and X. J. Huang, *Adv. Mater.*, 2009, **21**, 4593–4607.
- 5 Y. L. Liang, Z. L. Tao and J. Chen, *Adv. Energy Mater.*, 2012, **2**, 742–769.
- 6 P. Poizot, S. Laruelle, S. Grugeon, L. Dupont and J. M. Tarascon, *Nature*, 2000, **407**, 496–499.
- 7 G. Y. Zhao, N. Q. Zhang and K. N. Sun, *J. Mater. Chem. A*, 2013, **1**, 221–224.
- 8 L. J. Wang, B. Liu, S. H. Ran, L. M. Wang, L. N. Gao, F. Y. Qu, D. Chen and G. Z. Shen, *J. Mater. Chem. A*, 2013, **1**, 2139–2143.
- 9 Y. H. Xu, G. Q. Jian, M. R. Zachariah and C. S. Wang, *J. Mater. Chem. A*, 2013, **1**, 15486–15490.
- 10 H. L. Wang, L. F. Cui, Y. Yang, H. S. Casalongue, J. T. Robinson, Y. Y. Liang, Y. Cui and H. J. Dai, *J. Am. Chem. Soc.*, 2010, **132**, 13978–13980.
- 11 L. Zhou, H. B. Wu, T. Zhu and X. W. Lou, *J. Mater. Chem.*, 2012, **22**, 827–829.
- 12 P. Poizot, S. Laruelle, S. Grugeon and J. M. Tarascon, *J. Electrochem. Soc.*, 2002, **149**, A1212–A1217.
- 13 Y. Xia, Z. Xiao, X. Dou, H. Huang, X. H. Lu, R. J. Yan, Y. P. Gan, W. J. Zhu, J. P. Tu, W. K. Zhang and X. Y. Tao, *ACS Nano*, 2013, **7**, 7083–7092.
- 14 K. F. Zhong, B. Zhang, S. H. Luo, W. Wen, H. Li, X. J. Huang and L. Q. Chen, *J. Power Sources*, 2011, **196**, 6802–6808.
- 15 G. L. Xu, Y. F. Xu, H. Sun, F. Fu, X. M. Zheng, L. Huang, J. T. Li, S. H. Yang and S. G. Sun, *Chem. Commun.*, 2012, **48**, 8502–8504.
- 16 Y. M. Sun, X. L. Hu, W. Luo and Y. H. Huang, *J. Mater. Chem.*, 2012, **22**, 19190–19195.
- 17 X. W. Li, D. Li, L. Qiao, X. H. Wang, X. L. Sun, P. Wang and D. Y. He, *J. Mater. Chem.*, 2012, **22**, 9189–9194.
- 18 W. Luo, X. L. Hu, Y. M. Sun and Y. H. Huang, *ACS Appl. Mater. Interfaces*, 2013, **5**, 1997–2003.
- 19 X. Z. Wang, S. Qiu, G. X. Lu, C. Z. He, J. R. Liu, L. Q. Luan and W. Liu, *CrystEngComm*, 2014, **16**, 1802–1809.
- 20 S. B. Wang, Y. B. Ren, G. R. Liu, Y. L. Xing and S. C. Zhang, *Nanoscale*, 2014, **6**, 3508–3512.
- 21 X. W. Li, X. N. Shang, D. Li, H. W. Yue, S. Y. Wang, L. Qiao and D. Y. He, *Part. Part. Syst. Charact.*, 2014, DOI: 10.1002/ppsc.201400010.
- 22 H. L. Wang, Z. W. Xu, Z. Li, K. Cui, J. Ding, A. Kohandehghan, X. H. Tan, B. Zahiri, B. C. Olsen, C. M. B. Holt and D. Mitlin, *Nano Lett.*, 2014, **14**, 1987–1994.
- 23 G. Q. Zhang, H. B. Wu, H. E. Hoster and X. W. Lou, *Energy Environ. Sci.*, 2014, **7**, 302–305.
- 24 B. Sun, Z. X. Chen, H. S. Kim, H. Ahn and G. X. Wang, *J. Power Sources*, 2011, **196**, 3346–3349.
- 25 Y. M. Sun, X. L. Hu, W. Luo, F. F. Xia and Y. H. Huang, *Adv. Funct. Mater.*, 2012, **23**, 2436–2444.
- 26 Y. Li, Z. Y. Fu and B. L. Su, *Adv. Funct. Mater.*, 2012, **22**, 4634–4667.
- 27 A. Vu, Y. Q. Qian and A. Stein, *Adv. Energy Mater.*, 2012, **2**, 1056–1085.
- 28 Y. Ren, A. R. Armstrong, F. Jiao and P. G. Bruce, *J. Am. Chem. Soc.*, 2010, **132**, 996–1004.
- 29 W. B. Yue, C. Random, P. S. Attidekou, Z. X. Su, J. T. S. Irvine and W. Z. Zhou, *Adv. Funct. Mater.*, 2009, **19**, 2826–2833.
- 30 J. S. Chen, T. Zhu, X. H. Yang, H. G. Yang and X. W. Lou, *J. Am. Chem. Soc.*, 2010, **132**, 13162–13164.
- 31 X. W. Lou, D. Deng, J. Y. Lee and L. A. Archer, *J. Mater. Chem.*, 2008, **18**, 4397–4401.
- 32 D. H. Chen, F. Z. Huang, L. Cao, Y. B. Cheng and R. A. Caruso, *Chem. Eur. J.*, 2012, **18**, 13762–13769.
- 33 Q. L. Wu, J. C. Li, R. D. Deshpande, N. Subramanian, S. E. Rankin, F. Q. Yang and Y. T. Cheng, *J. Phys. Chem. C*, 2012, **116**, 18669–18677.
- 34 H. T. Zhou, M. A. Einarsrud and F. Vullum Bruer, *J. Power Sources*, 2013, **235**, 234–242.
- 35 X. C. Wang, J. C. Yu, C. Ho, Y. D. Hou and X. Z. Fu, *Langmuir*, 2005, **21**, 2552–2559.
- 36 X. N. Li, Y. C. Zhu, X. Zhang, J. W. Liang and Y. T. Qian, *RSC Adv.*, 2013, **3**, 10001–10006.
- 37 J. X. Zhu, D. Yang, X. H. Rui, D. H. Sim, H. Yu, H. H. Hng, H. E. Hoster, P. M. Ajayan and Q. Y. Yan, *Small*, 2013, **9**, 3390–3397.



## Graphic and text of the contents entry

### Facile template-free synthesis of 3D porous MnO/C microspheres with controllable pore size for high-performance lithium-ion battery anodes

Kai Su,<sup>a</sup> Chao Wang,<sup>b</sup> Honggang Nie,<sup>a</sup> Yan Guan,<sup>a</sup> Feng Liu<sup>\*a</sup> and Jitao Chen<sup>\*a</sup>



3D porous MnO/C anode materials with controllable pore size are synthesized for effectively optimizing the electrochemical performance.